Pressure effect in the antiperovskite phosphide superconductor $Sr(Pt_{0.9}Pd_{0.1})_3P$

Lifen Shi,[1,2] Pengtao Yang,[1] Teng Wang,[3] Pengfei Shan,[1] Ziyi Liu,[1] Shuxiang Xu,[1] Keyu Chen,[1] Ningning Wang,[1] Long Zhou,[1] Youwen Long,[1,2,5] Jianping Sun,[1,2] Gang Mu,[3,*] Yoshiya Uwatoko,[4] Bosen Wang,[1,2,5,†] and Jinguang Cheng[1,2,‡]

[1]*Beijing National Laboratory for Condensed Matter Physics and Institute of Physics, Chinese Academy of Sciences, Beijing 100190, China*

[2]*School of Physical Sciences, University of Chinese Academy of Sciences, Beijing 100190, China*

[3]*State Key Laboratory of Functional Materials for Informatics, Shanghai Institute of Microsystem and Information Technology, Chinese Academy of Sciences, Shanghai 200050, China and CAS Center for Excellence in Superconducting Electronics (CENSE), Shanghai 200050, China*

[4]*Institute for Solid State Physics, University of Tokyo, Kashiwanoha 5-1-5, Kashiwa, Chiba 277-8581, Japan*

[5]*Songshan Lake Materials Laboratory, Dongguan, Guangdong 523808, China*

(Received 21 March 2022; revised 13 May 2022; accepted 14 June 2022; published 30 June 2022)

We report a high-pressure study on the antiperovskite phosphide superconductor $Sr(Pt_{0.9}Pd_{0.1})_3P$. The superconducting transition temperature T_c decreases with a negative differential pressure coefficient, $d\ln T_c/dP \approx -0.052\,\mathrm{GPa}^{-1}$ ($dT_c/dP \approx -0.33\,\mathrm{K/GPa}$ for $P < 10\,\mathrm{GPa}$), which is a very high value for antiperovskite superconductors. We find that the upper critical field $\mu_0 H_{c2}(0)$ also decreases with increasing pressure, but the $\mu_0 H_{c2}(0)/k_B T_c$, e.g., $2\Delta_0[\pi N(E_F)]^{1/2}/k_B T_c$, is doubled from ~0.5–0.7 T/K at ambient pressure to ~1.2 T/K at 31.7 GPa. Our comparative studies on the dependences of T_c as functions of physical pressure versus chemical doping support that $Sr(Pt_{0.9}Pd_{0.1})_3P$ belongs to a phonon-mediated Bardeen-Cooper-Schrieffer-type superconductor with enhanced superconducting coupling strengths. The reduction of T_c with pressure should mainly originate from the decrease of the density of states at the Fermi level and the phonon-hardening effect. Our results shed some light on understanding the superconducting mechanisms of Pt-based antiperovskite superconductors.

DOI: 10.1103/PhysRevB.105.214529

I. INTRODUCTION

Polar metal usually involves the inversion symmetry breaking of crystal structure and polarized charges in real space [1]. Superconductors with polar structures are rare and have received increasing attention owing to exotic electronic states and possible unconventional pairing mechanisms [2–7]. The well-studied examples include the heavy-fermion superconductor $CePt_3Si$ [3], the Nb-doped ferroelectric $SrTiO_3$ [2] with intriguing quantum criticality, the superconducting SnP near the polar-nonpolar transition [6], and the enhancement of superconductivity (SC) in $MoTe_2$ near the polar structure instability [8]. Recently, Takayama *et al.* reported a new family of ternary Pt-based superconductors APt_3P (A = Sr, Ca, La) with an antipolar structure [9]. As shown in Fig. 1, the APt_3P crystallizes in a tetragonal structure (space group $P4/nmm$, No. 129) featured by the elongated distortions of the PPt_6 octahedron; the P ion is displaced with electric polarization along the c axis. The antiparallel polarizations cause $SrPt_3P$ to possess an antipolar nature. The APt_3P is centrosymmetric apart from the noncentrosymmetric heavy-fermion superconductor $CePt_3Si$ [3]. It was found that the superconducting transition temperature, T_c, of APt_3P 8.4, 6.6, and 1.5 K for A = Sr, Ca, and La, respectively [9]. These new superconducting materials share a similar crystal structure with the antiperovskitelike superconductors, including cubic $MgCNi_3$ ($T_c \approx 8\,\mathrm{K}$) [10], $CuNNi_3$ ($T_c \approx 3.2\,\mathrm{K}$) [11], and $SnSr_3O$ ($T_c \approx 5\,\mathrm{K}$) [12]. In addition, it has some connection with other Pt-based superconductors $SrPt_2As_2$ [13] and SrPtAs [14] with quasi-two-dimensional PtAs layers, which has thus rekindled the interest in these new superconductors.

Among the series of APt_3P, $SrPt_3P$ has attracted special attention because it not only shows the highest T_c among all the $5d$-based superconductors with antiperovskitelike structure, but also exhibits a larger ratio between superconducting gap Δ_0 and T_c, i.e., $2\Delta_0/k_B T_c \approx 5$, which indicates a strong coupling strength [9]. Such a large ratio is similar to cuprates [15,16] and iron-based unconventional superconductors [17–19]. Takayama *et al.* argued that the presences of low-lying phonons and the multiple Fermi-surface pockets are the key ingredients for the strong coupling with large $2\Delta_0/k_B T_c$ [9]. Kang *et al.* suggested that $SrPt_3P$ belongs to a strong-coupling phonon-mediated superconductor in which the superconducting charge carriers derived from the $pd\pi$ hybridization between Pt and P ions are coupled to the ab in-plane phonon modes (~5 meV) [20]. Such a conclusion of strong-coupling superconductivity in $SrPt_3P$ is supported by first-principles calculations [21]. However, nuclear magnetic resonance studies on $SrPt_3P$ indicated that it is a rather simple metal with spherically symmetric pairing configuration [22] and some other calculations revealed that APt_3P is a weak-coupling superconductor with three-dimensional

*mugang@mail.sim.ac.cn
†bswang@iphy.ac.cn
‡jgcheng@iphy.ac.cn

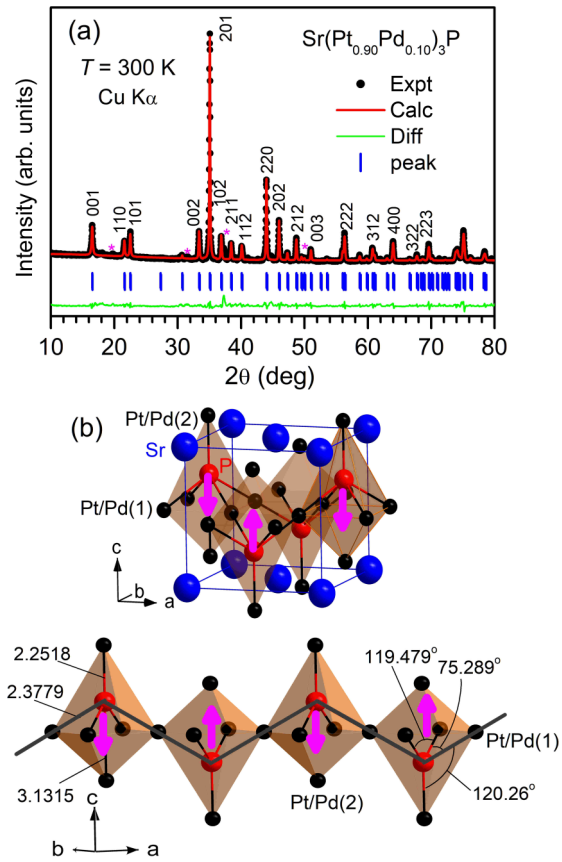

FIG. 1. (a) The Rietveld refinement on the x-ray powder diffraction (XRD) pattern of $Sr(Pt_{0.9}Pd_{0.1})_3P$. All the diffraction peaks can be indexed to the tetragonal structure with a tiny unknown phase as also found in Refs. [9,28,29]. (b) Crystal structure of $Sr(Pt_{0.9}Pd_{0.1})_3P$. It has an edge-sharing (Pt, Pd)$_6$P octahedron with the *c*-axis stretched distortion. The magenta arrows indicate the alternating polarization vector originated from the asymmetric Pt/Pd(2) positions.

Fermi surfaces [23]. Concerning these discrepancies, the studies on the lattice dynamics of $SrPt_3P$ pointed out that the enhanced electron-phonon coupling for the optical phonon modes (∼5.0 meV) is overestimated in calculations, which also supports $SrPt_3P$ to be a weak-coupling superconductor [24]. In addition, there exists some debate on whether the observed superconducting state is related with charge density wave (CDW); i.e., Chen *et al.* reported that the SC of $SrPt_3P$ is enhanced by CDW instability [25], while Subedi *et al.* excluded the CDW scenario and argued that the enhancement of superconducting pairing strength from La to Ca and Sr is associated with the changes in the electron-phonon matrix elements and low-frequency phonons [26]. In view of the above discrepancies about the superconducting mechanism, more comparative studies through high pressure and chemical substitutions are required.

Chemical doping and physical pressure are two effective methods to manipulate crystal and electronic structures and to reveal the physical parameters closely related to SC. In comparison to chemical doping, the application of physical pressure provides a clean and fine tuning knob without introducing lattice disorders. The comparative studies are helpful to uncover different contributions of physical quantities such as the lattice and carriers to the superconducting state. For parent $SrPt_3P$, a slight substitution of 4*d* Pd for Pt causes a decrease of T_c [27,28], which has been attributed to the enhancement of electron-electron correlations and the suppression of electron-phonon coupling and spin-orbit coupling; the hole doping by partially replacing P with Si also results in a monotonous decrease of T_c [29], which is contradictory to the theoretical calculations. In addition, we noticed that pressure can also affect the T_c of $SrPt_3P$ in such a way that firstly increases and then decreases in the pressure range of 0–1.7 GPa due to the decreasing of coupling strength [29]. However, the pressure range is rather limited. Based on these previous studies, electron-phonon coupling, electron-electron correlations, and density of states at the Fermi level are all important factors affecting the SC of APt_3P. In this regard, a further study on the evolution of these related parameters at elevated pressures is required to achieve a better understanding of SC in APt_3P.

We learned from the previous reports that the parent $SrPt_3P$ always contains some unknown impurities, which hinder the reliable analysis on experimental results, especially under high pressures. In contrast, those impurities can be substantially reduced in the Pd-substituted $Sr(Pt_{1-x}Pd_x)_3P$ superconducting samples with the same crystal structure [28]. Thus, $Sr(Pt_{0.9}Pd_{0.1})_3P$ with the highest T_c among this series of samples has been chosen as a good example to study the intrinsic pressure effect and to unveil the evolutions of electron-phonon coupling, electron-electron correlation, and the density of states at Fermi level under pressure [28]. In this work, we have investigated the superconducting properties of $Sr(Pt_{0.9}Pd_{0.1})_3P$ by measuring electrical transport under various pressures up to 31.7 GPa. Its T_c is found to decrease with increasing pressure. The comparative studies on the dependences of T_c on pressure and doping reveal that the negative pressure effect on T_c originates from the decrease in the density of states at the Fermi level and the phonon hardening under pressure.

II. EXPERIMENTAL METHODS

Polycrystalline $Sr(Pt_{0.9}Pd_{0.1})_3P$ samples were synthesized by the solid-state reaction method as reported elsewhere [27,28]. Phase purity of the obtained samples was examined by powder x-ray diffraction (XRD) using Cu $K\alpha_1$ radiation ($\lambda = 1.5406$ Å). The XRD pattern was refined with the Rietveld method by using FULLPROF software. Because the as-obtained sample is too loose to be cut into small pieces (the typical size of $0.20 \times 0.20 \times 0.60\,mm^3$) for high-pressure electrical measurements in a cubic anvil cell (CAC) apparatus, the synthesized polycrystalline samples wrapped with gold foil was cold pressed at 5 GPa for 35 min before high-pressure measurements. After the high-pressure treatment, we checked the XRD again and found no change in lattice parameters except for the broadening of some diffraction peaks. At ambient pressure (AP), electrical resistivity and Hall coefficient were measured by a standard four-probe method on the Quantum Design physical property measurement system ($0 \leqslant H \leqslant 9.0\,T$, $1.8 \leqslant T \leqslant 400\,K$); magnetic susceptibility

was also checked for ellipsoid sample and the applied field is basically parallel to its longest semiaxis.

The measurements of electrical resistivity and Hall coefficient under high pressure were performed in a palm-type CAC up to 11 GPa and a diamond anvil pressure cell (DAC) up to 31.7 GPa, respectively. In the CAC, glycerol was employed as the pressure transmitting medium (PTM), and the pressure values were estimated from the calibration curves determined at room temperature. In the DAC, a rhenium gasket was preindented to ∼33 μm and then a 100 μm diameter hole was drilled in the center using a laser drilling system, filled with soft material, KBr, as the PTM to keep a quasihydrostatic pressure. The rhenium gasket was covered with a *c*-BN epoxy as the insulating layer and resistivity was measured using the dc current in the van der Pauw configuration. The pressure was determined by the wavelength shift of the ruby $R1$ fluorescence line in the whole pressure range at room temperature. All the low-T measurements are carried out in a homemade ^{4}He cryostat equipped with a superconducting magnet system ($0 \leqslant H \leqslant 9.0$ T, $1.4 \leqslant T \leqslant 300$ K).

III. RESULTS AND DISCUSSION

Figure 1(a) shows the Rietveld refinement of a room-temperature powder XRD pattern for $Sr(Pt_{0.9}Pd_{0.1})_3P$ in the tetragonal $SrPt_3P$ structure (SG: $P4/nmm$, No. 129). The asterisks refer to some unknown impurities which were also observed in the parent $SrPt_3P$ by Takayama *et al.* and Hu *et al.* [9,27,28]. The obtained lattice parameters ($a = b = 5.8145$ Å, $c = 5.3689$ Å) are close to those reported in the literature [9]. A comparison with the values for pristine $SrPt_3P$ ($a = b = 5.809$ Å and $c = 5.383$ Å) indicates that the crystal lattice shows a slight shrinkage along the c axis and an expansion within the ab plane with increasing the Pd doping. The results indicate that the slight decrease of the c/a ratio upon Pd doping is advantageous for stabilizing the crystal structure so as to reduce the amount of impurities significantly [28]. The volume decreases slightly as a function of the Pd doping in the series of $Sr(Pt_{1-x}Pd_x)_3P$ for $0 \leqslant x \leqslant 0.1$, and then shows an increasing trend up to $x = 0.4$. Such a variation of $V(x)$ is abnormal regardless of comparing both the ion radius and metallic bond length of Pt and Pd. Besides, other isostructural $LaPd_3P$ and $CaPd_3P$ with smaller unit-cell volume are also stable without clear impurity [30,31], which indicates that the lower Pd doping is reliable and the induced chemical pressure stabilizes the crystal structure of the $SrPt_3P$ system. We thus chose to study the nearly single-phase $Sr(Pt_{0.9}Pd_{0.1})_3P$ sample under physical pressures. Figure 1(b) shows the crystal structure of slightly Pd-doped $Sr(Pt_{0.9}Pd_{0.1})_3P$, which can be described as the alternative stacking of the distorted $P(Pt/Pd)_6$ octahedra and Sr layers. The polarity of asymmetric distorted octahedra alternates within the ab planes, forming an antipolar pattern. In this case, the Pt/Pd(1)-5d bands contribute more to the electronic density of states near the Fermi level than the Pt/Pd(2)-5d and P-3p bands [23].

We first characterized the $Sr(Pt_{0.9}Pd_{0.1})_3P$ samples at AP by measuring the temperature dependences of electrical resistivity $\rho(T)$ and magnetic susceptibility $\chi(T)$. As shown in Fig. 2(a), $\rho(T)$ shows a metallic behavior with a sharp superconducting transition at low temperatures, which starts

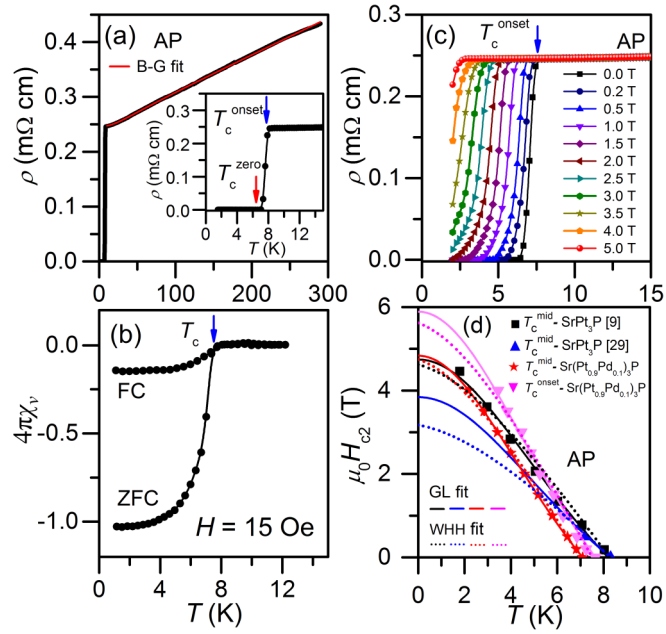

FIG. 2. (a), (b) Temperature dependences of electrical resistivity $\rho(T)$ at zero field and the superconducting volume $4\pi\chi_v(T)$ at a magnetic field of $\mu_0 H = 15$ Oe for $Sr(Pt_{0.9}Pd_{0.1})_3P$. Inset shows the enlarged view of low-T $\rho(T)$. The T_c^{onset} and T_c^{zero} are the onset and zero-resistivity temperature of the superconducting transition. The red solid line in (a) represents the fitting curve to the Bloch-Grüneisen (BG) formula. (c) $\rho(T)$ under various magnetic fields up to 5.0 T. (d) Temperature dependence of the upper critical field $\mu_0 H_{c2}(0)$ of $Sr(Pt_{0.9}Pd_{0.1})_3P$ and the fitting results by the Ginzburg-Landau (GL) equation and the Werthamer-Helfand-Hohenberg (WHH) model. The $\mu_0 H_{c2}(0)$ of $SrPt_3P$ is also included for comparison [9,28,29].

at ∼8.1 K and reaches zero resistivity at ∼7.2 K. Here, the T_c^{onset} is determined as the temperature deviating from the normal-state resistivity and T_c^{zero} is defined as the zero-resistivity temperature. These results agree well with the previous report [28] and thus confirm the high quality of our $Sr(Pt_{0.9}Pd_{0.1})_3P$ sample in this study. The superconducting transition temperature T_c^M determined from the $\chi(T)$ data in Fig. 2(b) is in perfect agreement with the $\rho(T)$ shown in Fig. 2(a). Bulk SC is also confirmed by the observation of large superconducting volume fractions of $4\pi\chi_v(2\,\mathrm{K}) \approx 100\%$ and 14.8% for the zero field cooled (ZFC) and field cooled (FC) processes, respectively. The difference of $4\pi\chi_v(T)$ between ZFC and FC suggests an enhanced magnetic flux pinning effect as the common feature of type-II superconductors.

Figure 2(c) shows the $\rho(T)$ curves under various magnetic fields up to 5 T, illustrating a gradual reduction of T_c with increasing magnetic field due to the magnetic pair-breaking effect. Here, we adopted the criteria of middle point and onset for the superconducting transition temperature, T_c^{mid} and T_c^{onset}, and plotted the temperature dependences of upper critical field $\mu_0 H_{c2}(T)$ in Fig. 2(d) together with those of $SrPt_3P$ for comparison. At first, these $\mu_0 H_{c2}(T)$ data can be well described by using the Ginzburg-Landau (GL) equation, i.e., $\mu_0 H_{c2}(T) = \mu_0 H_{c2}(0)(1-t^2)/(1+t^2)$, where $t = T/T_c$. As

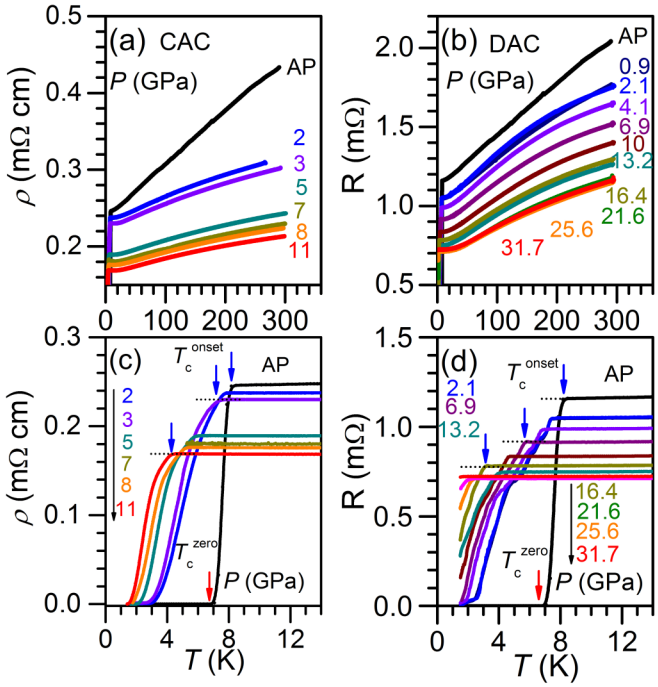

FIG. 3. Temperature dependence of electrical resistivity $\rho(T)$ under various pressures for $Sr(Pt_{0.9}Pd_{0.1})_3P$ in a cubic anvil pressure cell (CAC) and a diamond pressure cell (DAC): (a) $\rho(T)$ in CAC up to 11 GPa; (b) $\rho(T)$ in DAC up to 31.7 GPa. (c), (d) The enlarged superconducting transitions with the pressure; the blue and red arrows mark the onset temperature T_c^{onset} and zero-resistivity temperature T_c^{zero}, respectively.

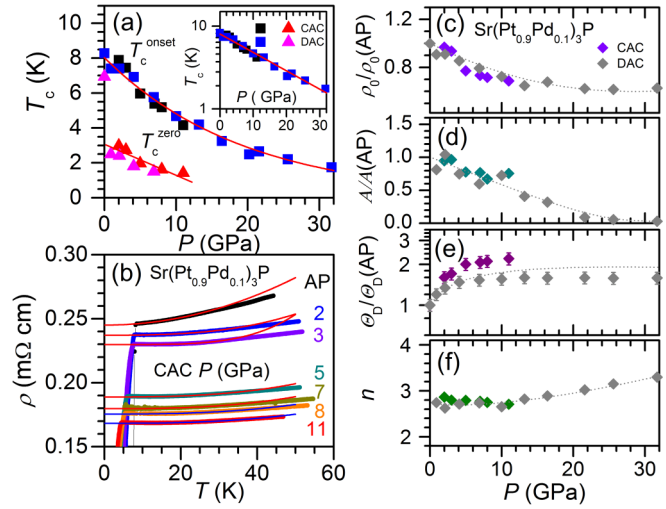

FIG. 4. (a) Pressure dependence of T_c^{onset} and T_c^{zero}. The inset shows the logarithmic scale of T_c^{onset}-P and the linear fit. The red lines in (a) across the data indicate the fitting results to the lnT_c-P plot; (b) Temperature dependence of $\rho(T)$ under various pressures and the fittings of normal-state resistivity by using $\rho = \rho_0 + AT^n$ with the residual resistivity ρ_0, the coefficient A, and the exponent n, respectively. Pressure dependence of characteristic parameters: (c) ρ_0/ρ_0(AP); (d) A/A(AP); (e) Θ_D/Θ_D(AP); (f) the n; the A is fitted with $n = 2$ and the dashed lines in (c–f) are guide for eyes.

shown in Fig. 2(d), the obtained $\mu_0 H_{c2}(0) = 4.83$ by using the T_c^{mid} for $Sr(Pt_{0.9}Pd_{0.1})_3P$ is slightly higher than those of two pristine $SrPt_3P$, i.e., ~3.84–4.69 T [9,22,28], which should be attributed to the magnetic flux pinning effect. For comparison, we also employed the Werthamer-Helfand-Hohenberg (WHH) model to extract the orbital-limiting $\mu_0 H_{c2}^{orb}(0)$, which are slightly smaller than those obtained from the GL fitting [32,33] for pristine $SrPt_3P$ and $Sr(Pt_{0.9}Pd_{0.1})_3P$. The large difference of $\mu_0 H_{c2}(0)$ for the two $SrPt_3P$ samples should be ascribed to the different sample qualities.

To trace the normal- and superconducting-state properties of $Sr(Pt_{0.9}Pd_{0.1})_3P$ under pressures, its $\rho(T)$ were measured in different pressure ranges by using the CAC (2–11 GPa) and DAC (0.9–31.7 GPa), respectively. As shown in Figs. 3(a) and 3(b), the normal-state $\rho(T)$ decreases monotonically with increasing pressure and the superconducting transition temperature T_c decreases gradually as depicted in Figs. 3(c) and 3(d). It is noted that the superconducting transition becomes broadened with increasing pressure, presumably due to the presence of shear stress or pressure inhomogeneity upon compression. As shown in Fig. 3(d), there is an additional step in some superconducting transitions under nonhydrostatic pressures in DAC, different from the smooth transitions under hydrostatic pressures in CAC. Pressure dependence of T_c^{onset} and T_c^{zero} determined from $\rho(T)$ are plotted in Fig. 4(a). We find that both T_c^{onset} and T_c^{zero} obtained from measurements in CAC and DAC almost coincide with each other, confirming the good reproducibility of pressure effect on $Sr(Pt_{0.9}Pd_{0.1})_3P$. A linear fitting to the $T_c(P)$ in the pressure range 0–10 GPa yields a negative differential pressure coefficient $dT_c/dP \approx -0.33$ K/GPa. It is noteworthy that this coefficient is the largest one among all the antiperovskitelike superconductors, as seen in Table I. At elevated pressures above 10 GPa, the reduction of $T_c(P)$ becomes slower with pressure. A careful examination of the pressure dependence of T_c reveals an exponential decay with a negative slope of $d\ln T_c/dP \approx -0.052\ \mathrm{GPa}^{-1}$ for $Sr(Pt_{0.9}Pd_{0.1})_3P$ in the whole pressure range, as shown in the inset of Fig. 4(a).

To gain more insight into the evolution of $T_c(P)$, the normal-state resistivity just above T_c is analyzed with the power-law formula, viz., $\rho = \rho_0 + AT^n$, where ρ_0 is the residual resistivity; the coefficient A and the exponent n are related to the density of state at Fermi level and the inelastic electron scattering, respectively. The polynomial fittings shown by the solid lines in Fig. 4(b) are performed from T_c to 30 K and n contains the information about electron-phonon scattering. Meanwhile, the quadratic temperature coefficient A extracted from a linear fit to the $(\rho-\rho_0)$ vs T^2 plot at the low-temperature limit reflects mainly the electron-electron interactions when most of the phonon modes are frozen. The obtained fitting parameters renormalized by their corresponding values at AP are compared in Figs. 4(c)–4(e). In a single-band model, the residual resistivity is simply expressed as $\rho_0 = (3\pi^2)^{1/3}(\hbar/e^2 l)/n_c^{2/3}$, where l and n_c represent the mean free path and carrier density, respectively [34]. Since the pressure-induced reduction of n_c is confirmed by the following Hall coefficient measurements, the monotonic decrease of ρ_0 here should be mainly attributed to the increase of l due to the reduction of grain boundary scattering upon compression. We also

TABLE I. Summary of the superconducting transition temperature T_c and its pressure coefficients for known antiperovskitelike superconductors.

Samples	T_c (K)	dT_c/dP (K/GPa)	$\mu_0 H_{c2}(0)$ (T)	Θ_D (K)	γ (mJ/mol K^2)	References
$MgNi_3C_x$	6.9–7.9	0.134–0.155	–	–	–	[39]
$MgNi_3C$	8.12	0.06	14.4	284	30.1	[40,41]
$CdNi_3C$	2.5-3.2	–	1.8–2.2	352	18.0	[41]
$CuNi_3N$	3.2	–	1.21	291	39.27	[11]
$ZnNi_3N_x$	3.0	–	0.96	336	13.0	[42]
$SnSr_3O$	5.0	–	0.44	–	–	[12]
AsV_3N	2.60	–0.013	2.79	364	22.0	[43,44]
$PV_3N_{0.9}$	5.6	–0.19	3.49	489	19.5	[43,44]
$(Ca_{0.6}Sr_{0.4})Pt_3P$	3.54	–0.15(1)	2.53	184	6.24	[31]
$(Ca_{0.25}Sr_{0.75})Pt_3P$	0.32	–	0.032	242	3.61(9)	[31]
$SrPt_3P$	8.40	–	5.80	190	12.7	[9]
$CaPt_3P$	6.60	–	–	218	17.4	[9]
$LaPt_3P$	1.50	–	–	–	6.70	[9]
$SrPt_3P$	8.35	0.12 ($<$ 1 GPa)	–	190	–	[29]
$SrPd_3P$	0.06	–	–	–	–	[30]
$LaPd_3P$	0.28	–	0.306	267	6.06(4)	[31]
$SrPt_3P_{0.8}Si_{0.2}$	7.80	–	–	–	7.73	[29]
$SrPt_3P$	8.4	–	$<$5.0	–	13.54	[28]
$Sr(Pt_{0.9}Pd_{0.1})_3P$	7.60	–0.33	4.83-6.0	135.3	–	This work

find that the $A/A(\mathrm{AP})$ value decreases strongly by nearly one order at 20 GPa and then changes weakly. Generally, the A value is proportional to the square of the Sommerfeld coefficient by the Kadowaki-Woods relationship and thus reflects the density of states at Fermi level $N(E_F)$ [35]. Thus, the decrease in the $A/A(\mathrm{AP})$ signals the reduction of $N(E_F)$, which correlated positively with the evolution of T_c. The estimated exponent n shows a weak pressure dependence by increasing from 2.6–2.7 to 3.0–3.2 in the studied pressure range, which is different from the typical value of $n = 2(5)$ for electron-electron (electron-phonon) scatterings. The observed $n \approx 3$ deviating from the Landau Fermi liquid in $Sr(Pt_{0.9}Pd_{0.1})_3P$ under pressure suggests enhanced phonon scatterings. Besides, the evolution of Debye temperature Θ_D was obtained by fitting the $\rho(T)$ curve with the Bloch-Grüneisen (BG) formula [36]. At AP, as shown in Fig. 2(a), the well-fitted BG formula gives $\Theta_D \approx 135.3$ K in $Sr(Pt_{0.9}Pd_{0.1})_3P$, which is lightly lower than that of ~190 K in $SrPt_3P$. In order to eliminate the influence of pressure variation and electron contribution at low temperature, we roughly estimated the Θ_D at various pressures. As suggested, for $T > 0.5\Theta_D$ ($\Theta_D \approx 190$ K in $SrPt_3P$ and ≈218 K in $CaPt_3P$), the temperature dependence of high-temperature resistivity can be described by $\rho(T) \approx A'T/4M\Theta_D^2 \approx BT$, where A' and M represent the characteristic parameter and the atomic mass, respectively. As shown in Fig. 4(e), we find that the value of the $\Theta_D(P)/\Theta_D^{\mathrm{AP}}$ ratio increases monotonously from 1.0 at AP to 1.50 at 31.7 GPa, which is evidence of phonon hardening upon compression and is consistent with the increasing tendency of $\Theta_D \approx 190$ K in $SrPt_3P$ to $\Theta_D \approx 218$ K in $CaPt_3P$. Our results are also consistent with some theoretical predictions [21,37,38].

To further understand the evolution of SC, we measured the temperature dependence of resistivity under various magnetic fields at each pressure. As shown in Figs. 5(a)–5(f), T_c^{onset} moves to lower temperatures gradually with increasing magnetic fields. By choosing T_c^{onset} and $T_c^{90\%-R_n}$ (temperature of 90% normal-state resistance R_n), the T_c–$\mu_0 H_{c2}$ data are plotted in Fig. 6(a) and zero-temperature $\mu_0 H_{c2}(0)$ is obtained by using the empirical GL fitting as shown by the solid lines. For comparison, we also employed the WHH model to extract the orbital-limiting $\mu_0 H_{c2}^{\mathrm{orb}}(0)$ based on the initial slope of $\mu_0 H_{c2}(T)$ around T_c. Although slight differences are noticed for the obtained $\mu_0 H_{c2}(0)$ values in these two methods, they display similar pressure dependences. As illustrated in Fig. 6(b), the obtained $\mu_0 H_{c2}(0)$ values decrease monotonically with increasing pressure from ~6 to ~3 T.

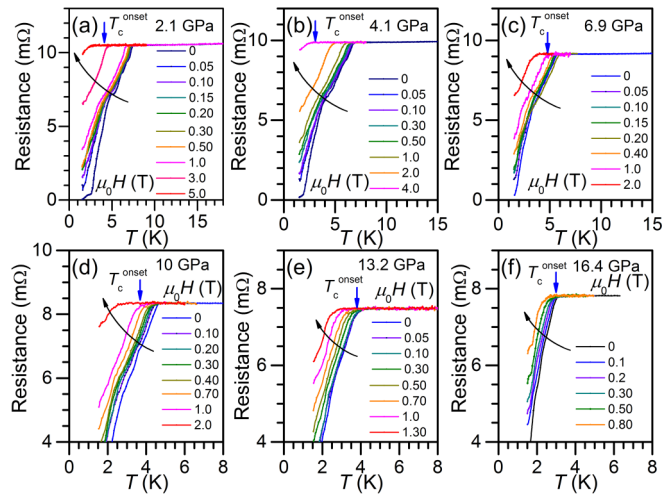

FIG. 5. Temperature dependence of resistance $R(T)$ under various magnetic fields and selected pressures. The T_c^{onset} represents the superconducting transition temperature and the arrows show the changing trends.

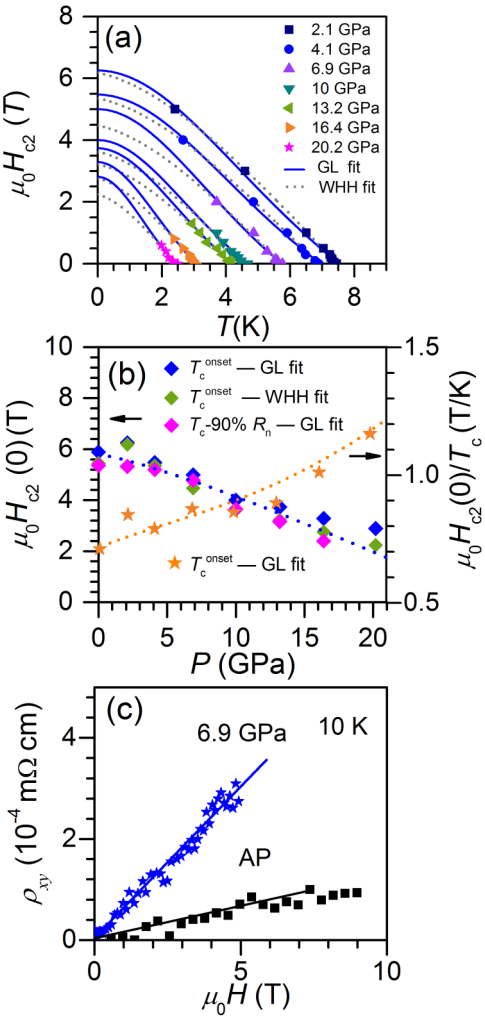

FIG. 6. (a) Temperature dependence of the upper critical field $\mu_0 H_{c2}(T)$ under various pressures up to 20.2 GPa in a diamond pressure cell. The solid and dashed lines represent the GL and WHH fittings, respectively. (b) The pressure dependences of $\mu_0 H_{c2}(0)$ (on the left) and $\mu_0 H_{c2}(0)/T_c$ (on the right). The dashed lines show the changing trends. (c) Hall resistivity $\rho_{xy}(H)$ at 10 K under AP and 6.9 GPa.

Such a moderate (∼50%) reduction of $\mu_0 H_{c2}(0)$ cannot be rationalized by considering only the change of $N(E_F)$, which is expected to undergo a significant decrease with increasing pressure as indicated by the reduction (∼10%) of quadratic temperature coefficient A in Fig. 4(d). Instead, the superconducting energy gap Δ_0 might be strengthened by pressure according to the relationship $\mu_0 H_{c2}(0) \approx 2\Delta_0[\pi N(E_F)]^{1/2}$. To substantiate this point, we have obtained the $\mu_0 H_{c2}(0)/T_c$, e.g., $2\Delta_0[\pi N(E_F)]^{1/2}/T_c$, which is found to increase from ∼0.5–0.7 T/K at AP to ∼1.2 T/K at 20 GPa as shown in Fig. 6(b). Considering the decrease of the $N(E_F)$, we deduce that the increment of $2\Delta_0/k_B T_c$ is much stronger than that of $\mu_0 H_{c2}(0)/T_c$, e.g., 2–3 times. Based on these results, we may conclude that the superconducting coupling strengths of $Sr(Pt_{0.9}Pd_{0.1})_3P$ are enhanced although its T_c is reduced by pressure. Figure 6(c) shows the Hall resistivity $\rho_{xy}(H)$ at 10 K at AP and 6.9 GPa. For both pressures, the $\rho_{xy}(H)$ shows a nearly linear H dependence. The positive slope of

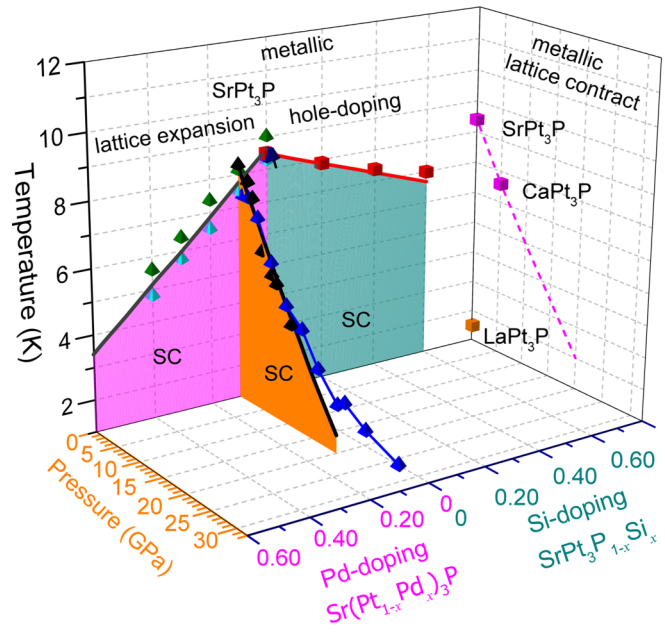

FIG. 7. Temperature-pressure phase diagram of superconductor $Sr(Pt_{0.9}Pd_{0.1})_3P$. The dependence of superconducting transition temperatures on chemical-doping level is summarized for $Sr(Pt_{1-x}Pd_x)_3P$ [27,28], $SrPt_3P_{1-x}Si_x$ [29], $SrPt_3P$, $CaPt_3P$, and $LaPt_3P$ [9]; for $SrPr_3P$ and $CaPt_3P$, the chemical pressure is converted into an equal amount of physical pressure according to the bulk elastic modulus and the volume changes. The lines across the data are a guide for the eyes.

$\rho_{xy}(H)$ at AP and 6.9 GPa indicates that the hole-type carriers dominate the electrical transport in $Sr(Pt_{0.9}Pd_{0.1})_3P$. The Hall coefficient obtained at 6.9 GPa (∼2.09×10^{-3} cm^3/C) is about 4.5 times larger than that at AP (∼4.32×10^{-4} cm^3/C), which corresponds to the decrease of the dominant carrier concentration.

Based on the above results, a comprehensive temperature-pressure-composition phase diagram was constructed for $SrPt_3P$. As shown in Fig. 7, both the electron doping (replacing Sr/Ca with La) and the hole doping ($SrPt_3P_{1-x}Si_x$) reduce the T_c value with increasing the doping level. This feature seems to contradict the previous theoretical predictions considering only the change of carrier density of states $N(E_F)$ [23]. At the same time, we also find that both positive chemical pressure (from $SrPt_3P$ to $CaPt_3P$) and physical pressure [$Sr(Pt_{0.9}Pd_{0.1})_3P$] suppress the superconducting transition temperature, which is different from the observation of a monotonic increase of T_c in $SrPt_3P$ at 0–1.0 GPa originated from the increase of Debye temperature [29]. Interestingly, the volume increase as a function of the Pd doping in $Sr(Pt_{1-x}Pd_x)_3P$ results in a monotonic reduction of T_c [27,28]. According to the previously reported bulk modulus of $SrPt_3P$ and $CaPt_3P$ [37,38], the equivalent pressure is about 5 GPa and the pressure coefficient is about $dT_c/dP \approx -0.36$ K/GPa if considering only the volume shrinkage from $SrPt_3P$ to $CaPt_3P$. This estimation seems to be equivalent to the observed $dT_c/dP \approx -0.33$ K/GPa for $Sr(Pt_{0.9}Pd_{0.1})_3P$ at $P <$ 10 GPa in the present work. However, the reduction of T_c with a slight change of volume in the case of $Sr(Pt_{1-x}Pd_x)_3P$ does not conform to the above scenario, which indicates that

other factors also play an important role in determining the evolution of T_c with pressure. Nonetheless, our comparative studies based on high-pressure and chemical-doping effects support that $Sr(Pt_{0.9}Pd_{0.1})_3P$ belongs to a phonon-mediated Bardeen-Cooper-Schrieffer (BCS)-type superconductor with enhanced coupling strength by pressure.

Finally, we discuss briefly some important issues. Firstly, the SC of $SrPt_3P$ seems to be optimized and its T_c is readily suppressed by the application of tuning parameters including the isovalent/hole doping, lattice expansion/shrinkage. According to the previous studies, the effect of spin-orbit coupling of heavy-element Pt and Pd is negligible [20,21,26], which makes $SrPt_3P$ a trivial electronic system with dominated electron-electron and electron-phonon couplings. The change of lattice parameters and electronic structures and the couplings between them should be the key to understanding the above phase diagrams. Under pressure, the decrease of T_c is mainly attributed to the decrease of density of states at the Fermi level, although pressure drives a phonon hardening, which increases Debye temperature and the lattice vibration ending frequency. This is consistent with the previous theoretical and experimental studies [29]. Meanwhile, the enhanced electron-electron scatterings may reduce the T_c according to the previous reports [28].

The second issue is the superconducting coupling strengths under pressure. As mentioned above, our results support that the SC of $Sr(Pt_{0.9}Pd_{0.1})_3P$ is phonon mediated and the $2\Delta_0/k_BT_c$ ratio increases more quickly than the $\mu_0H_{c2}(0)/T_c$ ratio with the pressure, indicating the enhancement of superconducting coupling strength under pressure despite the reduction of T_c. It has been shown that $SrPt_3P$ at AP is a strong- or moderate-coupling superconductor with $2\Delta_0/k_BT_c$ larger than 3.52 for the conventional weak-coupling BCS superconductors. The enlarged superconducting gap value or the contributions of high-frequency optical phonons may contribute to the enhanced electron-phonon coupling. However, the previous studies suggested that the zero-temperature superconducting gap ~1.55 meV is overestimated to be ~5.0 meV and leaves little space for the strong coupling limited SC [24]. Further studies to directly probe the superconducting coupling strength are needed to clarify these discrepancies.

Last, but not least, the role of antipolar structure in $Sr(Pt_{0.9}Pd_{0.1})_3P$ on the superconducting pairing is proposed. In tetragonally distorted SnP, the superconducting state emerges when its polar structure associated with the charge transfer from Sn to P is suppressed by pressure, which indicates strong competitions between the polar and superconducting states [6]. Similarly, the T_c of $SrPd_3P$ rises suddenly from 0.05–0.32 K to 3.5–4 K accompanying the tetragonal-orthorhombic structure phase transition, which can be attributed to the suppression of the polar structure and/or noncentrosymmetry [30]. Meanwhile, some theoretical calculations also implied that the coupling between the superconducting carriers and in-plane phonon modes is dominated, which does not break the antipolar nature of $SrPt_3P$ [20]. However, the polar structure may compete with the in-plane pairing electronic states and reduces the T_c. Following this idea, high T_c may appear if the antipolar structure could be suppressed, which needs more follow-up experimental studies.

IV. CONCLUSION

In summary, we performed a comprehensive high-pressure study on the antiperovskite phosphide superconductor $Sr(Pt_{0.9}Pd_{0.1})_3P$. Its $T_c(P)$ decreases with increasing pressure in a relatively large slope of $d\ln T_c/dP \approx -0.052\,GPa^{-1}$ ($dT_c/dP \approx -0.33\,K/GPa$ for $P < 10\,GPa$), which is a very high value for antiperovskite superconductors. The upper critical field $\mu_0H_{c2}(0)$ also reduces but the $\mu_0H_{c2}(0)/k_BT_c$ ratio increases presumably due to the enhanced superconducting coupling strength. Our studies support $Sr(Pt_{0.9}Pd_{0.1})_3P$ as a phonon-mediated BCS superconductor and the evolution of T_c with pressure mainly originates from the decrease in the density of states at Fermi level and phonon hardening.

ACKNOWLEDGMENTS

This work is supported by the Beijing Natural Science Foundation (Grants No. Z190008 and No. Z200005), the National Key Research and Development Program of China (Grants No. 2018YFA0305700, No. 2018YFA0305800, No. 2016YFA0300404, No. 2018YFE0202600, and No. 2016YFA0300504), the National Natural Science Foundation of China (Grants No. 11921004, No. 11834016, No. 11874400, No. 51171177, No. 11674326, No. 11874357, No. 11774423, and No. 11822412), the Strategic Priority Research Program and Key Research Program of Frontier Sciences of Chinese Academy of Sciences (Grants No. XDB25000000, No. XDB33000000, and No. QYZDB-SSWSLH013), and the Youth Promotion Association of CAS (Grant No. 2018010).

L.S. and P.Y. contributed equally to this work.

[1] V. M. Edelstein, Phys. Rev. Lett. **75**, 2004 (1995).

[2] A. Leitner, D. Olaya, C. T. Rogers, and J. C. Price, Phys. Rev. B **62**, 1408 (2000).

[3] E. Bauer, G. Hilscher, H. Michor, C. Paul, E. W. Scheidt, A. Gribanov, Y. Seropegin, H. Noel, M. Sigrist, and P. Rogl, Phys. Rev. Lett. **92**, 027003 (2004).

[4] S. E. Rowley, L. J. Spalek, R. P. Smith, M. P. M. Dean, M. Itoh, J. F. Scott, G. G. Lonzarich, and S. S. Saxena, Nat. Phys. **10**, 367 (2014).

[5] I. Belopolski, D. S. Sanchez, Y. Ishida, X. Pan, P. Yu, S. Y. Xu, G. Q. Chang, T. R. Chang, H. Zheng, N. Alidoust, G. Bian, M. Neupane, S. M. Huang, C. C. Lee, Y. Song, H. J. Bu, G. H. Wang, S. S. Li, G. Eda, H. T. Jeng *et al.*, Nat. Commun. **7**, 13643 (2016).

[6] M. Kamitani, M. S. Bahramy, T. Nakajima, C. Terakura, D. Hashizume, T. Arima, and Y. Tokura, Phys. Rev. Lett. **119**, 207001 (2017).

[7] P. A. Volkov and P. Chandra, Phys. Rev. Lett. **124**, 237601 (2020).

[8] H. Takahashi, T. Akiba, K. Imura, T. Shiino, K. Deguchi, N. K. Sato, H. Sakai, M. S. Bahramy, and S. Ishiwata, Phys. Rev. B. **95**, 100501(R) (2017).

[9] T. Takayama, K. Kuwano, D. Hirai, Y. Katsura, A. Yamamoto, and H. Takagi, Phys. Rev. Lett. **108**, 237001 (2012).
[10] T. He, Q. Huang, A. P. Ramirez, Y. Wang, K. A. Regan, N. Rogado, M. A. Hayward, M. K. Haas, J. S. Slusky, K. Inumara, H. W. Zandbergen, N. P. Ong, and R. J. Cava, Nature (London) **411**, 54 (2001).
[11] B. He, C. Dong, L. H. Yang, X. C. Chen, L. H. Ge, L. B. Mu, and Y. G. Shi, Supercond. Sci. Technol. **26**, 125015 (2013).
[12] M. Oudah, A. Ikeda, J. N. Hausmann, S. Yonezawa, T. Fukumoto, S. Kobayashi, M. Sato, and Y. Maeno, Nat. Commun. **7**, 13617 (2016).
[13] K. Kudo, Y. Nishikubo, and M. Nohara, J. Phys. Soc. Jpn. **79**, 123710 (2010).
[14] Y. Nishikubo, K. Kudo, and M. Nohara, J. Phys. Soc. Jpn. **80**, 055002 (2011).
[15] B. Keimer, S. A. Kivelson, M. R. Norman, S. Uchida, and J. Zaanen, Nature (London) **518**, 179 (2015).
[16] P. Fournier, Physica C **514**, 314 (2015).
[17] H. Hosono and K. Kuroki, Physica C **514**, 399 (2015).
[18] J. P. Sun, K. Matsuura, G. Z. Ye, Y. Mizukami, M. Shimozawa, K. Matsubayashi, M. Yamashita, T. Watashige, S. Kasahara, Y. Matsuda, J. Q. Yan, B. C. Sales, Y. Uwatoko, J. G. Cheng, and T. Shibauchi, Nat. Commun. **7**, 12146 (2016).
[19] K. Kothapalli, A. E. Bohmer, W. T. Jayasekara, B. G. Ueland, P. Das, A. Sapkota, V. Taufour, Y. Xiao, E. Alp, S. L. Bud'ko, P. C. Canfield, A. Kreyssig, and A. I. Goldman, Nat. Commun. **7**, 12728 (2016).
[20] C. J. Kang, K. H. Ahn, K. W. Lee, and B. I. Min, J. Phys. Soc. Jpn. **82**, 053703 (2013).
[21] R. Szczęśniak, A. P. Durajski, and Ł. Herok, Phys. Scr. **89**, 125701 (2014).
[22] T. Shiroka, M. Pikulski, N. D. Zhigadlo, B. Batlogg, J. Mesot, and H.-R. Ott, Phys. Rev. B **91**, 245143 (2015).
[23] I. A. Nekrasov and M. V. Sadovskii, JETP Lett. **96**, 227 (2012).
[24] D. A. Zocco, S. Krannich, R. Heid, K.-P. Bohnen, T. Wolf, T. Forrest, A. Bosak, and F. Weber, Phys. Rev. B **92**, 220504(R) (2015).
[25] H. Chen, X. F. Xu, C. Cao, and J. H. Dai, Phys. Rev. B **86**, 125116 (2012).
[26] A. Subedi, L. Ortenzi, and L. Boeri, Phys. Rev. B **87**, 144504 (2013).
[27] K. K. Hu, B. Gao, Q. C. Ji, Y. H. Ma, H. Zhang, G. Mu, F. Q. Huang, C. B. Cai, and X. M. Xie, Front. Phys. **11**, 117403 (2016).
[28] K. K. Hu, B. Gao, Q. C. Ji, Y. H. Ma, W. Li, X. G. Xu, H. Zhang, G. Mu, F. Q. Huang, C. B. Cai, X. M. Xie, and M. H. Jiang, Phys. Rev. B. **93**, 214510 (2016).
[29] BenMaan I. Jawdat, B. Lv, X. Zhu, Y. Xue, and C.-w. Chu, Phys. Rev. B. **91**, 094514 (2015).
[30] A. Iyo, H. Fujihisa, Y. Gotoh, S. Ishida, H. Ninomiya, Y. Yoshida, H. Eisaki, H. T. Hirose, T. Terashima, and K. Kawashima, Inorg. Chem. **59**, 12397 (2020).
[31] A. Iyo, I. Hase, H. Fujihisa, Y. Gotoh, S. Ishida, H. Ninomiya, Y. Yoshida, H. Eisaki, H. T. Hirose, T. Terashima, and K. Kawashima, Inorg. Chem. **60**, 18017 (2021).
[32] N. R. Werthamer, E. Helfand, and P. C. Hohenberg, Phys. Rev. **147**, 295 (1966).
[33] K. Y. Ma, K. Gornicka, R. Lefevre, Y. Yang, H. M. Rønnow, H. O. Jeschke, T. Klimczuk, and F. O. von Rohr, ACS Mater. Au **1**, 55 (2021).
[34] T. Muramatsu, N. Takeshita, C. Terakura, H. Takagi, Y. Tokura, S. Yonezawa, Y. Muraoka, and Z. Hiroi, Phys. Rev. Lett. **95**, 167004 (2005).
[35] K. Kadowaki and S. B. Woods, Solid State Commun. **58**, 507 (1986).
[36] D. Cvijovic, Theor. Math. Phys. **166**, 37 (2011).
[37] X. Q. Zhang, G. J. Li, Y. Cheng, and G. F. Ji, Philos. Mag. **96**, 399 (2016).
[38] X. Q. Zhang, Z. Y. Zeng, Y. Cheng, and G. F. Guang, RSC Adv. **6**, 27060 (2016).
[39] H. D. Yang, S. Mollah, W. L. Huang, P. L. Ho, H. L. Huang, C. J. Liu, J. Y. Lin, Y. L. Zhang, R. C. Yu, and C. Q. Jin, Phys. Rev. B **68**, 092507 (2003).
[40] G. Garbarino, M. Monteverde, M. Nunez-Regueiro, C. Acha, R. Weht, T. He, K. A. Regan, N. Rogado, M. Hayward, and R. J. Cava, Physica C **408–410**, 754 (2004).
[41] M. Uehara, T. Yamazaki, T. Kôri, T. Kashida, Y. Kimishima, and I. Hase, J. Phys. Soc. Jpn. **76**, 034714 (2007).
[42] M. Uehara, A. Uehara, K. Kozawa, T. Yamazaki, and Y. Kimishima, Physica C **470**, S688 (2010).
[43] B. S. Wang, J. G. Cheng, K. Matsubayashi, Y. Uwatoko, and K. Ohgushi, Phys. Rev. B **89**, 144510 (2014).
[44] B. S. Wang and K. Ohgushi, Sci. Rep. **3**, 3381 (2013).